



Cu/ZnO/CeO₂ Supported on MOF-5 as a Novel Catalyst for the CO₂ Hydrogenation to Methanol: A Mechanistic Study on the Effect of CeO₂ and MOF-5 on Active Sites

Seyed Alireza Vali¹ · Javier Moral-Vico¹ · Xavier Font¹ · Antoni Sánchez¹

Received: 10 October 2023 / Accepted: 9 December 2023
© The Author(s) 2024

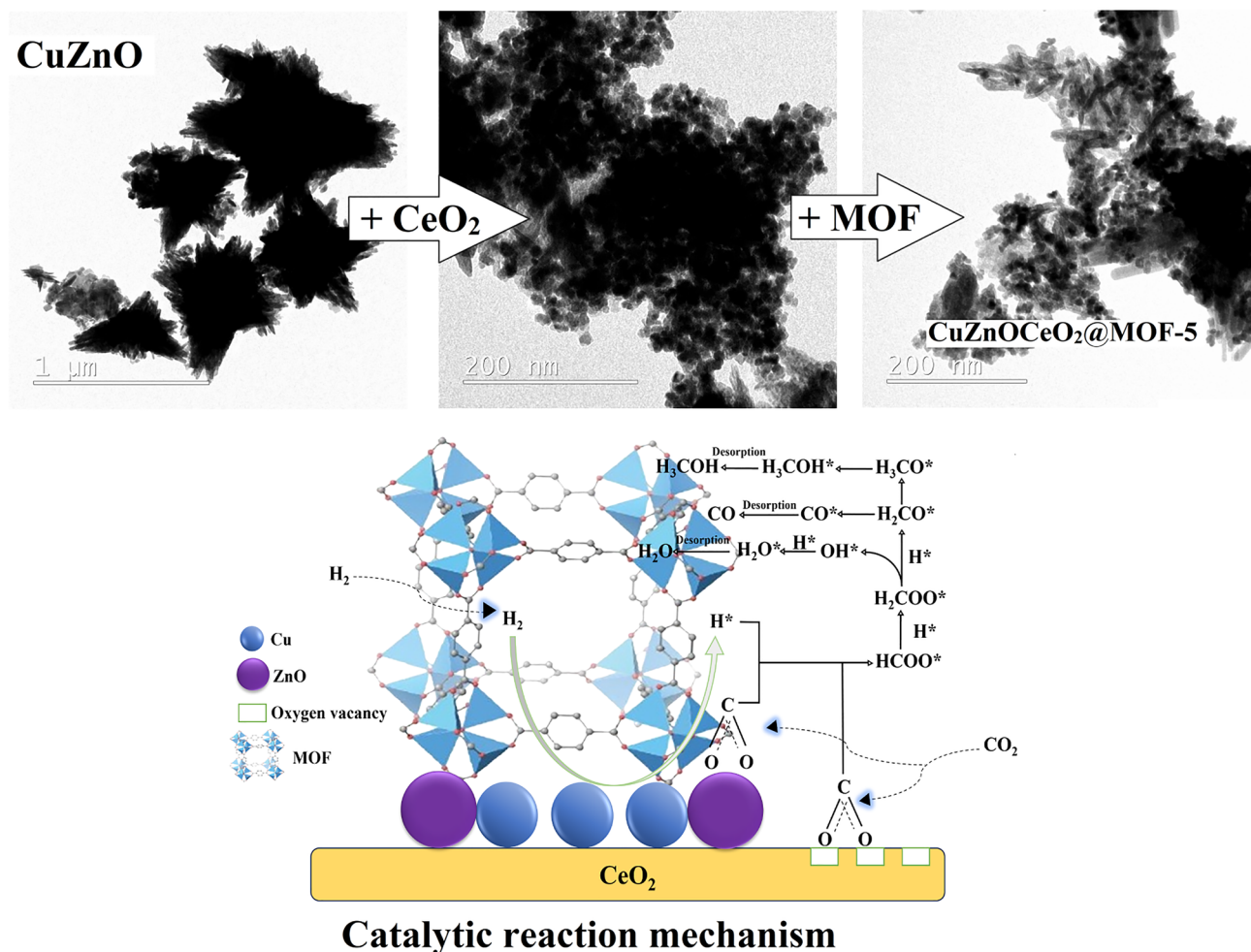
Abstract

Cu/ZnO/CeO₂ nanocomposite was supported on metal organic framework (MOF-5) to enhance active sites dispersion and control the nanoparticles agglomeration during synthesis through strong metal-support interactions. The incorporation of MOF-5 alleviated the obstacle facing the commercial ternary Cu/ZnO/Al₂O₃ regarding low surface area due to nanoparticles agglomeration. In addition, Cu/ZnO/CeO₂@MOF-5 gave higher methanol selectivity than the commercial catalyst which can be accounted for by the interfacial sites generated between MOF-5 and Cu/ZnO which favour methanol synthesis over carbon monoxide through regulating the intermediates bonding energies. CeO₂ as support for Cu/ZnO nanoparticles was also compared with commercial support and showed to have led to smaller particle size and superior dispersion of Cu active sites as well. Cu/ZnO/CeO₂@MOF-5 resulted in methanol STY of 23.3 mg g_{cat}⁻¹ h⁻¹ and selectivity of 79% at mild reaction temperature (260 °C) and pressure (10 bar). Two different MOFs including cerium based MOF and ZIF-8 demonstrated inferior performance compared to MOF-5.

✉ Seyed Alireza Vali
Seyedalireza.vali@uab.cat

¹ Composting Research Group (GICOM), Department of Chemical, Biological and Environmental Engineering, Universitat Autònoma de Barcelona, 08193 Bellaterra, Barcelona, Spain

Graphical Abstract



Keywords Methanol synthesis · Cu-based catalyst · Metal–organic framework (MOF) · Metal–support interaction · CO₂ hydrogenation · Cu/ZnO/CeO₂

1 Introduction

The current worldwide environmental crisis has been increased by the exploitation of fossil fuels that results in an increase of carbon dioxide concentration in the atmosphere. This has incentivized the research of new clean and sustainable energy resources as promising alternatives [1–4]. Carbon dioxide capture and storage (CCS) process and chemical transformation have been considered as effective methods for the removal of carbon dioxide and the production of renewable energy [5, 6]. Hydrogenation of carbon dioxide to methanol has been especially emphasized as a significant process since methanol is an intrinsically potential fuel and a raw material for fuel cells, as well as being a precursor for the

synthesis of other higher hydrocarbons and alternative fuels [7]. Nonetheless, there still exist obstacles to overcome as far as direct hydrogenation of carbon dioxide to methanol is concerned, due to the high thermodynamic stability and low reactivity of carbon dioxide that results in an unfavorable carbon dioxide conversion [8, 9]. Additionally, carbon monoxide produced from the reverse water gas shift reaction (RWGS) is unavoidable, leading to an undesirable methanol selectivity [10]. Hence, the research on finding highly efficient catalysts has gained popularity to improve the efficiency of carbon dioxide hydrogenation to methanol.

Cu-based catalysts have emerged and have been investigated extensively for methanol synthesis from carbon dioxide hydrogenation [11–14]. Although Cu alone can

work independently as catalyst for methanol synthesis, its activity has been significantly boosted by the incorporation of ZnO, due to enhancement in the dispersion of Cu NPs (nanoparticles) as well as the Cu/ZnO interface that acts as active site for spillover of hydrogen and carbon dioxide adsorption [11, 15–17]. Indeed, there are several hypotheses that explain how ZnO promotes the Cu catalytic activity including: (1) gas-dependent morphological changes of Cu on ZnO [18, 19]; (2) support-induced strain in Cu [20]; (3) ZnO_x species/layers covering part of the Cu NPs [19, 21–23], often regarded as strong metal-support interaction (SMSI), and (4) Cu/ZnO synergy owing to the incorporation of Zn atoms into the Cu surface steps [24]. However, Cu/ZnO-based catalysts suffer from significant drawbacks of having low active surface area as well as the sintering of metal phase under the reaction conditions. Therefore, Al₂O₃ has been used as a support for Cu/ZnO nanocomposites to eliminate the aforementioned obstacles to some extent. Hence, Cu/ZnO/Al₂O₃ has been utilized as the commercial catalyst for methanol synthesis from syngas (CO/CO₂/H₂) at elevated pressures (50 to 100 bar) and temperature (200–300 °C) [25]. Although Cu/ZnO/Al₂O₃ is well optimized for methanol synthesis from syngas, it demonstrates inadequacy in the conversion of a feed of CO₂ and H₂ to methanol owing to the competing RWGS reaction [26] and the water-induced deactivation [27–29]. Hence, other metal oxides such as ZrO₂ [30, 31], TiO₂ [32], In₂O₃ [33], La₂O₃ [34], Mo₂C [35] and La₂O₂CO₃ [36] have been reported to have enhanced both catalytic activity and selectivity of Cu-based catalysts. Furthermore, CeO₂ has been reported to improve the methanol selectivity of Cu-based catalyst more effectively than other supports such as ZrO₂. This is mainly attributed to the be the oxygen vacancies generated on the Cu/CeO₂ interface due to the metal-support interactions that enhance Cu dispersion as well as the stabilization of key reaction intermediates [37, 38] leading to higher selectivity. Thus, the simultaneous incorporation of both ZnO and CeO₂ in a Cu catalyst resulted in higher methanol selectivity compared to Cu/ZnO and Cu/CeO₂, which is explained by Zn promoting the Cu surface area and CeO₂ inhibiting the RWGS reaction [39, 40].

Metal–Organic Frameworks (MOFs) have gained interest in catalytic applications over the last decades owing to their extraordinary characteristics [41–44]. However, MOFs, when utilized alone, do not have considerable catalytic sites for the methanol synthesis from carbon dioxide hydrogenation. However, they can serve as a framework for the incorporation of metallic NPs to enhance their catalytic activity and overcome the

obstacles that metal-based catalysts encounter including low surface area, agglomeration, low dispersion and sintering during the reaction. In addition, the interface created as a result of the interactions between the metal catalyst and the MOF support has proved to be excellent active sites for methanol synthesis from CO₂ hydrogenation [45, 46]. For instance, Yang et al. [46] presented the catalyst Cu/ZnO_x@UiO-66 and established that the facilitation in the formation of Cu/ZnO_x interface, which is the responsible site for the excellent performance of the catalysts, was attributed to the presence of ultra-small nanoparticles confined in UiO-66. Moreover, the interaction of the metal sites of the catalyst with the metal nodes of the MOF might lead to the higher performance of the catalyst. For instance, Yaghi et al. [47] attempted to encapsulate Cu NPs in UiO-66 for the catalytic conversion of carbon dioxide to methanol. They demonstrated that the interaction between Cu NPs and Zr metal nodes led to the formation of the Cu–Zr interfaces promoting the performance of carbon dioxide adsorption and activation. In this work, three novel catalysts by supporting Cu/ZnO/CeO₂ on MOF-5, Cerium-based MOF, and ZIF-8 for methanol synthesis from carbon dioxide hydrogenation are presented. MOF-5 showed the highest performance in terms of methanol STY and selectivity compared to the other two. It is assumed that the high capacity of MOF-5 for gas adsorption facilitates the adsorption H₂ and CO₂ (the reaction reactants) and therefore enhances the catalytic activity. Another assumption is that the interaction between the metal nodes of the MOF-5 and active sites of Cu/ZnO/CeO₂ can contribute to the dispersion of Cu as main catalytic active sites. Our hypotheses were further confirmed via characterizations analyses. In addition, the reaction conditions (pressure of 10 bar and temperature 260–300 °C) of this study were relatively moderate compared to other studies previously mentioned with pressures ranging from 30 to 50 bar [45–47], which confirmed the applicability of the catalyst Cu/ZnO/CeO₂@MOF-5 under mild conditions. Characterizations techniques including scanning electron microscope (SEM), transmission electron microscope (TEM), energy dispersive X-ray spectroscopy (EDX), N₂ adsorption, and X-ray diffraction (XRD) were employed to observe the changes in Cu phase, dispersion, average size and specific surface area. Besides, CeO₂ was also compared with commercial catalyst and showed superior performance as support for Cu/ZnO since it led to smaller Cu particle size and dispersion through strong metal-support interaction.

2 Experimental

2.1 Catalyst Preparation

2.1.1 Materials

Zinc nitrate hexahydrate ($\text{Zn}(\text{NO}_3)_2 \cdot 6\text{H}_2\text{O}$), copper nitrate trihydrate ($\text{Cu}(\text{NO}_3)_2 \cdot 3\text{H}_2\text{O}$), cerium nitrate hexahydrate ($\text{Ce}(\text{NO}_3)_3 \cdot 6\text{H}_2\text{O}$), triethylamine, N,N-Dimethylformamide, ammonium hydroxide (NH_4OH), H_2BDC (Benzene-1,4-dicarboxylic acid), aluminium oxide (Al_2O_3) and sodium carbonate (Na_2CO_3), and commercial ZIF-8 were purchased from Merck (Barcelona, Spain). The purity of all reagents is higher than 99.0% and they were used as received. The carbon dioxide and hydrogen mixture with a molar ratio of 1:3, respectively, was provided by Carbueros Metálicos, S.A. (Barcelona, Spain).

2.1.2 Synthesis of ZnO

ZnO nanoparticles were synthesized via precipitation method [17]. Typically, $\text{Zn}(\text{NO}_3)_2 \cdot 6\text{H}_2\text{O}$ (15 g, 0.2 mol) was dissolved in 250 mL of de-ionized (DI) water for 30 min and then transferred to a 500 mL Scharlau Minireactor HME-R/500 with mechanical stirring and heating. Then a solution of Na_2CO_3 (0.2 M) was added dropwise using a peristaltic pump (rate of 5 mL/min) and the mixture was stirred at 120 rpm and 60 °C for 2 h, then washed with deionized water (DI) water and centrifuged 3 times (10 min and 6000 rpm). The obtained slurry was dried at 105 °C overnight.

2.1.3 Synthesis of CeO_2

CeO_2 nanoparticles were prepared through precipitation method [32]. Typically, $\text{Ce}(\text{NO}_3)_3 \cdot 6\text{H}_2\text{O}$ (1.25 g, 0.287 mmol) was dissolved in 50 mL of de-ionized (DI) water. Then, a solution of NH_4OH (5%, v/v) was added dropwise until the pH of the solution reached 10. The mixture was aged for 3 h, then washed with DI to set the solution pH at 7 and then centrifuged (10 min and 6000 rpm). The obtained slurry was dried at 80 °C for 12 h. Finally, the dried sample was calcined at 400 °C for 3 h.

2.1.4 Synthesis of Cu/ZnO/CeO_2

Furthermore, certain amounts of previously prepared ZnO and CeO_2 were dispersed in 50 mL DI water for 2 h using an ultrasonic bath. Next, the suspension was transferred to the previously described 500 mL Scharlau Minireactor HME-R/500, and then a certain amount (to keep the ratio of Cu/Zn/Ce as 3/3/1) of $\text{Cu}(\text{NO}_3)_2 \cdot 3\text{H}_2\text{O}$ was added and

the mixture was left to be stirred for 30 min at 60 °C and 120 rpm. Then, sodium carbonate (1M) solution was added dropwise to reach a pH of 10. The resultant mixture was aged for 2 h at 60 °C while stirring at 120 rpm. Afterwards, the final slurry was washed with DI water and centrifuged 3 times and dried at 105 °C overnight. Cu/ZnO and $\text{Cu/ZnO/Al}_2\text{O}_3$ were synthesized with the same procedure under the same conditions with the same ratios of Cu, Zn, and Al as in Cu/ZnO/CeO_2 .

2.1.5 Synthesis of MOFs

The MOFs were prepared according to the methods available in literature [48, 49]. For the synthesis of MOF-5, triethylamine (3.4 mL) was added dropwise to a N,N-dimethylformamide (DMF) solution (100 mL) containing $\text{Zn}(\text{NO}_3)_2 \cdot 6\text{H}_2\text{O}$ (1.786 g, 6 mmol) and H_2BDC (0.5 g, 3 mmol) under strong stirring at room temperature and aged for 2 h. The resultant solution was then washed with DMF and centrifuged 3 times. Finally, the slurry was dried at 90 °C for 12 h to obtain the final nano particles. The same procedure was used for the Ce-based MOF using $\text{Ce}(\text{NO}_3)_3 \cdot 6\text{H}_2\text{O}$ as Ce precursor.

2.1.6 Synthesis of $\text{Cu/ZnO/CeO}_2\text{@MOF-5}$

0.5 mmol of the as-synthesized MOF-5 was dispersed in 50 mL of DI water for 2 h using an ultrasonic bath. In addition, certain amounts of as-prepared ZnO and CeO_2 were dispersed in 50 mL of DI water for 2 h using an ultrasonic bath. The solution containing Zn and Ce was transferred to the 500 mL Scharlau Minireactor HME-R/500 while a defined amount (to keep the ratio of Cu/Zn/Ce as 3/3/1) of $\text{Cu}(\text{NO}_3)_2 \cdot 3\text{H}_2\text{O}$ was added and the mixture and allowed to be stirred for 30 min at 60 °C and 120 rpm. Then, the MOF suspension was added and the resultant mixture was also stirred at the same conditions for 30 min. Finally, sodium carbonate (1M) was added dropwise to the solution to reach a pH of 10. The resultant mixture was aged for 2 h at 60 °C while stirring at 120 rpm. The resultant slurry was the washed with DI water and centrifuged 3 times and dried at 105 °C overnight to obtain the final nanoparticles. Cu/ZnO/CeO_2 supported on the other two MOFs were prepared with a similar procedure.

2.2 Catalyst Characterization

Scanning electron microscopy (SEM) (Merlin FE-SEM) equipped with an energy dispersive x-ray spectroscopy (EDS) detector (EDS Oxford LINCA X-Max) was used to determine the size distribution and elemental composition of the nanomaterials. Transmission electron microscopy (TEM) (Hitachi H-7000) was also employed to analyse the size and

morphology of the NPs. Specific surface area, total pore volume and pore size distribution were measured by means of nitrogen adsorption/desorption at $-196\text{ }^{\circ}\text{C}$ using an ASAP 2020 Micrometrics Inc (BET analyser). Before analysis, samples were degassed at $80\text{ }^{\circ}\text{C}$ for 20 h. To determine the crystalline nature of the catalyst, powder X-ray diffraction (XRD) measurements were performed. The XRD patterns were recorded in a diffractometer (Panalytical X'Pert) using Cu-K α radiation ($\lambda = 1.5418\text{ \AA}$). The measurements were made at room temperature at a range of $0\text{--}80^{\circ}$ on 2θ with a step size of 0.02° . All XRD results were analysed with the simulation of the NPs obtained using the HighScore Plus software. The crystal sizes were calculated using Scherrer equation (Eq. 1):

$$D = \frac{K\lambda}{\beta \cos\theta} \quad (1)$$

where D is mean size of the ordered (crystalline) domains, K is Scherrer constant, λ is the X-ray wavelength, β is the line broadening at half the maximum intensity (FWHM), and θ is the Bragg angle (in radian).

2.3 Catalytic Experiments

To investigate the catalytic activity of the catalysts for the hydrogenation of carbon dioxide to methanol, they were fixed in a continuous vertical fixed bed tubular stainless-steel reactor (5.25 mm internal diameter and 8.90 cm length) resulting in a volume of 1.92 cm^3 , with a certain amount of catalyst (25 mg, 3 mm bed height). The catalyst particles was placed between two thin layers of glass wool inside the reactor. The catalytic experiments were carried out at low pressures of 10 and 15 bar and at a flow rate of 10 mL/min and at temperatures ranging from 260 to $300\text{ }^{\circ}\text{C}$. The gas samples were collected using sampling bags (SKC FlexFoil PLUS Sample Bag) and the collected methanol was analysed on a gas chromatograph (Shimadzu GC-2010) with a flame ionization detector (FID) and helium as the carrier gas. The software used was Chromeleon to determine the concentrations of chemical compounds, with the inlet temperature of $260\text{ }^{\circ}\text{C}$ and the flow of 50 mL/min, and the detector temperature was $280\text{ }^{\circ}\text{C}$. An Agilent 7890B GC System chromatograph was employed to measure carbon monoxide and carbon dioxide and methane, using a thermal conductivity detector (TCD), and helium as the carrier gas with an inlet temperature of $120\text{ }^{\circ}\text{C}$, an inlet flow of 20 mL/min, and a detector temperature of $150\text{ }^{\circ}\text{C}$. The software employed was Agilent OpenLAB CDS ChemStation (Version A.01.04). To study the catalytic activity of each samples, methanol space time yield (STY) and selectivity were calculated. In the selectivity calculations, only carbon monoxide was counted as the by-product since there were no other products

observed, and the STY and selectivity of methanol were calculated using the following Eqs. 2 and 3:

$$\text{CH}_3\text{OH STY} \left(\frac{\text{mg}}{\text{g}_{\text{cat}} \times \text{h}} \right) = \left(\frac{\text{Mass of methanol (mg) formed}}{W_{\text{cat}} (\text{g}) \times \text{Hour}} \right) \quad (2)$$

$$\text{CH}_3\text{OH Selectivity} (\%) = \left(\frac{\text{moles of methanol formed}}{n[\text{CO}_2]_{\text{in}} - n[\text{CO}_2]_{\text{out}}} \right) \times 100 \quad (3)$$

while $n[\text{CO}_2]_{\text{in}}$ is the amount (in moles) of CO₂ at the reactor inlet, $n[\text{CO}_2]_{\text{out}}$ stands for the amount of CO₂ at the reactor outlet and W_{cat} is the weight of catalyst used (g).

3 Results

3.1 Catalysts Characterization

3.1.1 XRD

The crystallographic structure of the catalyst samples of Cu/ZnO, Cu/ZnO/Al₂O₃, Cu/ZnO/CeO₂, Cu/ZnO/CeO₂@Ce-MOF and Cu/ZnO/CeO₂@MOF-5 were analyzed using XRD and presented in Fig. 1. The diffraction peaks appeared at $2\theta = 35.38^{\circ}$, 38.86° , 48.86° , 61.63° , and 65.89° are attributed to CuO phase [50]. In addition, ZnO phase was observed at diffraction angles of 31.74° , 34.42° , 36.35° , 47.39° , 56.53° , 62.95° and 68.04° [51]. As can be seen in Fig. 1, due to the incorporation of Al₂O₃, two diffraction peaks at 11.64° and 23.42° appeared, corresponding to ZnAl hydrotalcite phase formed with the formula $\text{Zn}_{0.67}\text{Al}_{0.33}(\text{OH})_2(\text{CO}_3)_{0.165} \cdot 0.5\text{ H}_2\text{O}$ [52]. ZnAl hydrotalcites have been patented as precursors of catalysts for the polyethoxylation of alcohols [53]. However, according to the STY and selectivity results presented later, the presence of this phase did not positively contribute to the production of methanol in the hydrogenation of CO₂ reaction, but led the reaction towards the production of carbon monoxide, which can be observed by the comparison of selectivity results of Cu/ZnO and Cu/ZnO/Al₂O₃. Additionally, the peaks appeared at diffraction angles of 28.49° , 33.02° and 76.54° are ascribed to the formation of CeO₂ in crystalline phase, which is in agreement with the literature [54]. Furthermore, the peaks appeared at diffraction angles of 8.4° , 10.6° and 18.1° as presented in Fig. 1 show the formation of Ce-based MOF as reported in literature [55]. Moreover, the intense peaks that appeared at diffraction angles of 6.8° , 9.7° , 13.7° and 15.4° and a few weak peaks in the range of 20 to 60° indicate the formation of MOF-5 in the crystalline phase [48, 49]. The comparison between the XRD pattern for MOF-5 and the catalyst Cu/ZnO/CeO₂@MOF-5 shows that the crystalline structure of MOF is maintained during the preparation of the catalyst Cu/ZnO/CeO₂@MOF-5 (Fig. 1b). Scherrer equation was applied to the data

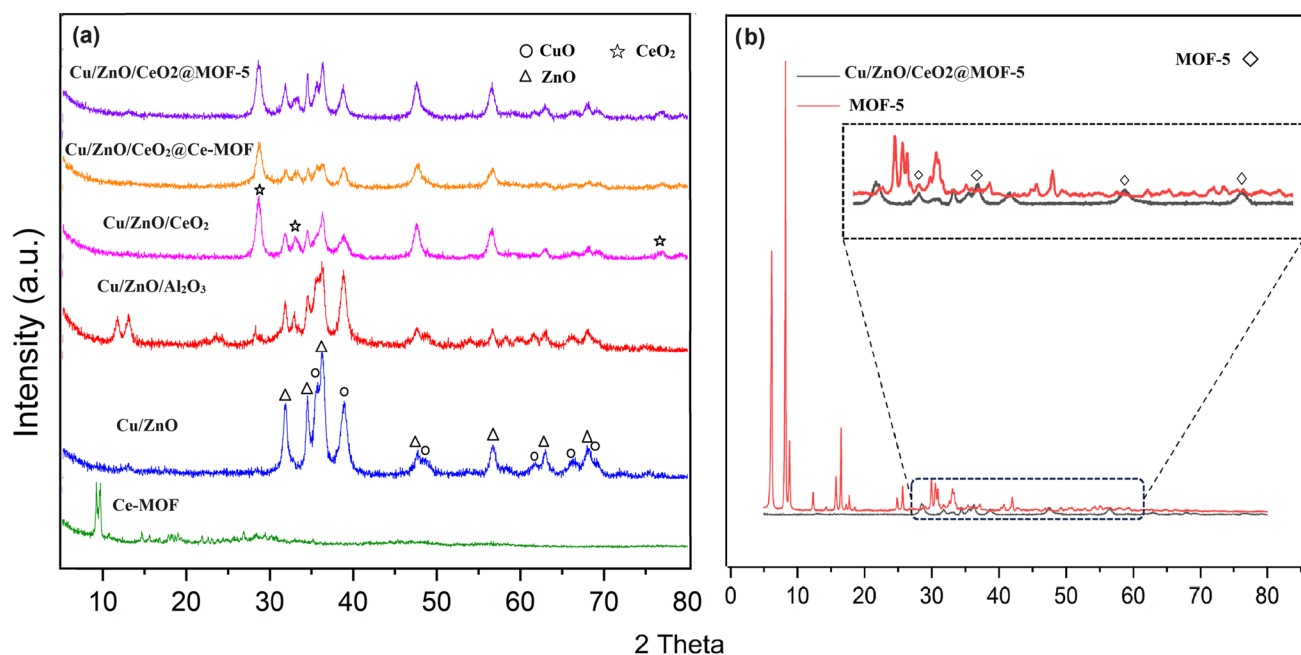


Fig. 1 X-ray diffraction patterns of the catalyst samples

Table 1 Textural and crystal properties of the catalyst samples

Samples	BET surface area (m ² /g)	Total pore volume (cm ³ /g)	Average pore size (nm)	Average CuO crystal size (nm) ^a
Cu/ZnO	38	0.167	16.28	24.13
Cu/ZnO/Al ₂ O ₃	41	0.237	13.7	17.84
Cu/ZnO/CeO ₂	50	0.142	8.48	17.16
Cu/ZnO/CeO ₂ @Ce-MOF	67	1.04	31	15.72
Cu/ZnO/CeO ₂ @MOF-5	69	0.2	15.45	15.27

^aCalculated using Scherrer equation from X-ray diffraction data

extracted from XRD analysis to calculate the average size of CuO particles in each catalyst sample, and the results are presented in Table 1. As observed, the XRD patterns of all the catalyst samples demonstrate the identical characteristic peaks corresponding to CuO and ZnO, suggesting that the addition of neither metal oxides of Al₂O₃ or CeO₂, nor MOFs did not disturb the crystallinity of Cu/ZnO composites. However, the intensity and broadness of the peaks are affected by these additions, which will be further discussed.

3.1.2 BET Analysis

Nitrogen adsorption–desorption isotherms of the catalyst samples are shown in Fig. 2. The catalysts showed a type IV isotherm and a H₃ type hysteresis loop in the relative pressure (P/P^0) range of 0.2–1.0, corresponding to the characteristics of mesoporous materials [56]. The hysteresis loop

in the relative pressure (P/P^0) is narrowed down to 0.5–1.0 and 0.8–1.0 for Cu/ZnO/CeO₂ and Cu/ZnO/CeO₂@MOF-5, respectively, which indicates the presence of micropores and mesopores in these catalysts. Furthermore, the pore size distribution curves corresponding to all samples are displayed in Fig. 3, while the specific surface area, average pore size and total pore volume of all the catalyst samples are presented in Table 1. As can be seen, the magnitude of specific area of the samples increases as follows: Cu/ZnO/CeO₂@MOF-5 > Cu/ZnO/CeO₂@Ce-MOF > Cu/ZnO/CeO₂ > Cu/ZnO/Al₂O₃ > Cu/ZnO. These results indicate that the incorporation of CeO₂ within CuZnO nanocomposite increases the specific area of the Cu/ZnO nanocomposite more significantly than when Al₂O₃ is used as support. In case of MOFs incorporation with the Cu/ZnO/CeO₂ nanocomposite, higher specific surface areas are observed, which are attributed to

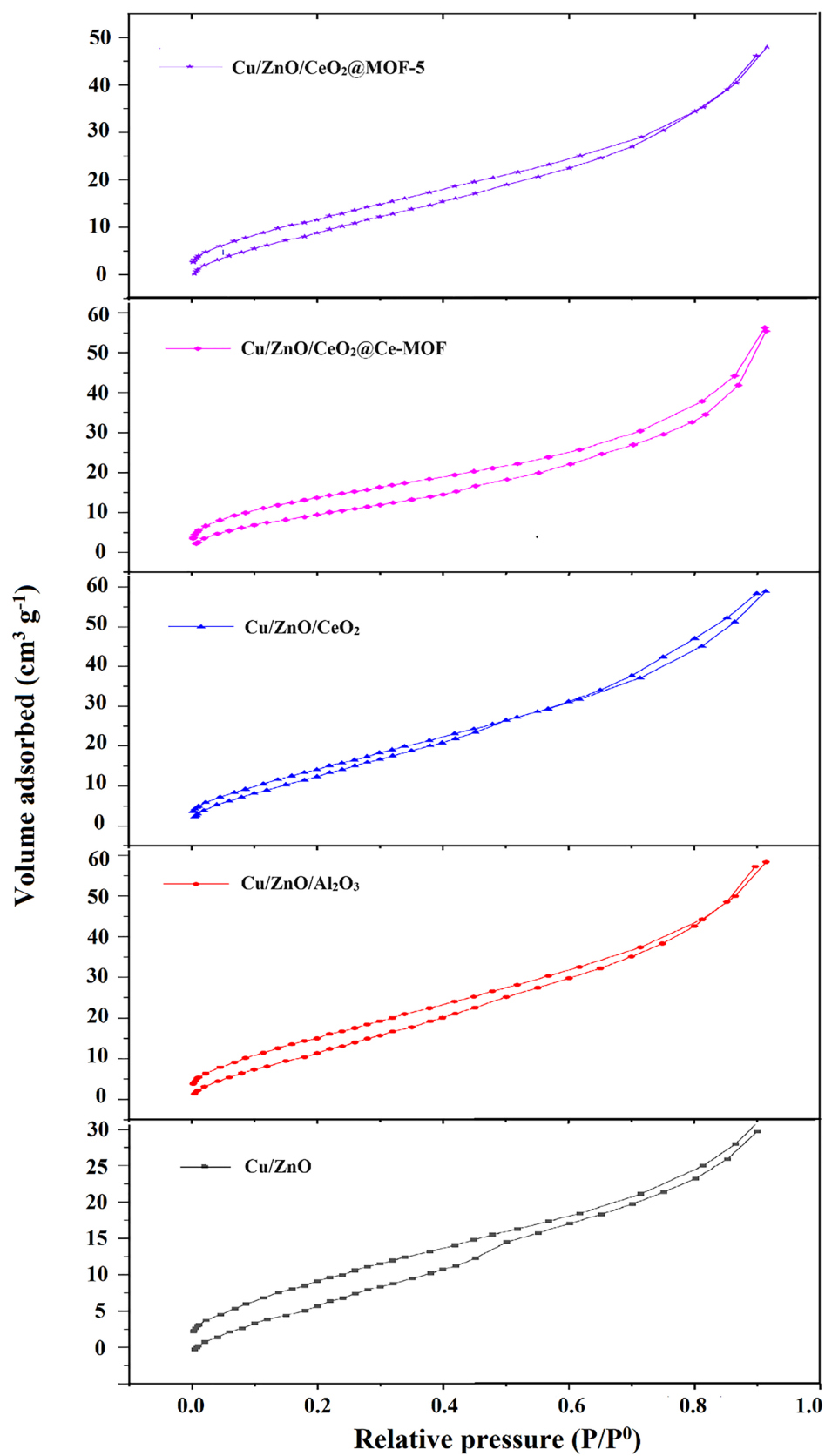
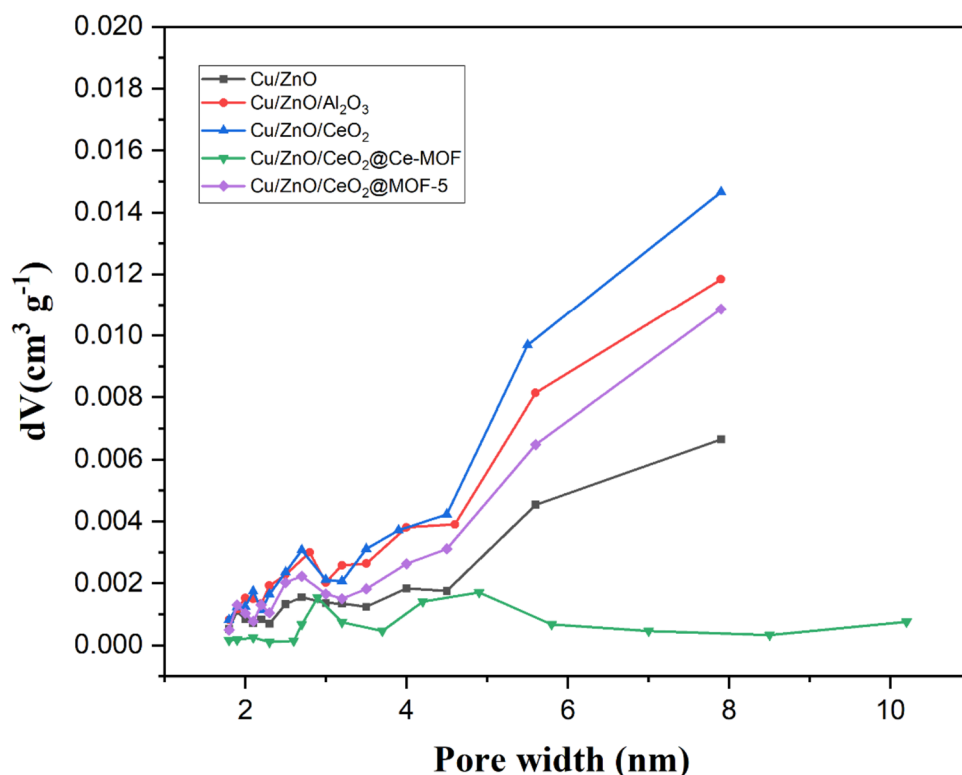
Fig. 2 BET isotherm for the catalyst samples

Fig. 3 Pore size distribution curves for catalyst samples



highly porous structure of MOFs as well as higher Cu dispersion and therefore higher Cu available surface area.

3.1.3 SEM and TEM

Scanning electron microscopy (SEM) as well as Transmission electron microscopy (TEM) analyses for all catalyst samples were carried out to observe the shape, morphology and size distribution as presented in Fig. 4. In addition to these observations, elemental composition of the samples were obtained from EDS analysis as presented in Table 2. Furthermore, elemental distribution mapping of the catalyst samples were obtained from EDS analysis to further facilitate the establishment of the positive effect that the incorporation of CeO₂ and MOFs have on the dispersion of Cu nanoparticles in the catalysts. The elemental distribution mapping results of the catalyst samples are shown in Fig. 5, in which (a–e) are corresponding to Cu/ZnO, Cu/ZnO/Al₂O₃, Cu/ZnO/CeO₂, Cu/ZnO/CeO₂@Ce-MOF and Cu/ZnO/CeO₂@MOF-5, respectively. The colors cyan, red, and yellow are ascribed to oxygen, copper and zinc, respectively. As can be seen, the elemental distribution mapping can facilitates the observation of CeO₂ and MOF effects on the dispersion of Cu and Zn in the catalyst composite, which will be discussed further.

3.2 Catalytic Reaction Performance

To evaluate the activity of the catalyst samples, the hydrogenation of carbon dioxide to methanol was performed under three different reaction conditions: (1) temperature 260 °C and pressure 10 bar (2) temperature 300 °C and pressure 10 bar (3) temperature 300 °C and pressure 15 bar. The results of the catalysts hydrogenation reaction in terms of methanol space–time yield (STY) and selectivity are shown in Table 3 and Fig. 6.

The results showed that the catalyst Cu/ZnO/CeO₂@MOF-5 performed better in terms of methanol STY and selectivity than the catalyst supported by the other two MOFs. Methanol STY for the samples increases with the following order: Cu/ZnO/CeO₂@MOF-5 > Cu/ZnO/CeO₂@Ce-MOF > Cu/ZnO/CeO₂ > Cu/ZnO/Al₂O₃ > Cu/ZnO. Comparing the methanol STY for samples with the specific surface area results presented before, it can be confirmed that the use of CeO₂ as a support for Cu/ZnO nanocomposite contributes significantly to its catalytic activity as Cu/ZnO/CeO₂ had higher surface area than the commercial Cu/ZnO/Al₂O₃. Moreover, the comparison between the STY and selectivity results of Cu/ZnO/CeO₂ and Cu/ZnO/CeO₂ supported by MOF-5 can reveal the positive impact that MOFs incorporation had on the catalytic activity.

As can be seen in Fig. 6, methanol STY corresponding to MOFs, when alone, were negligible (0.7–1.5 mg g_{cat}^{−1} h^{−1}), signifying that although MOFs, when used as supports,

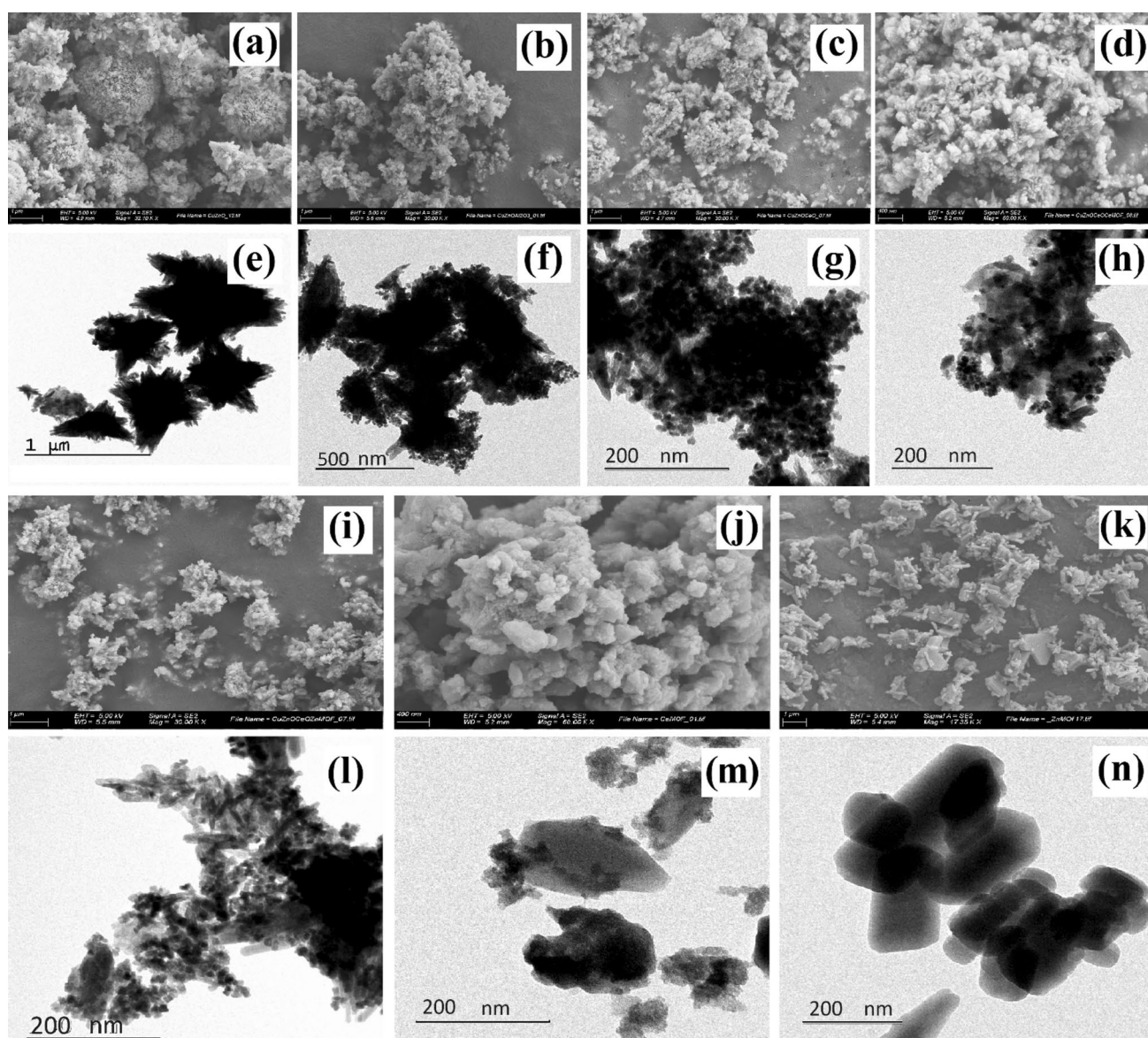


Fig. 4 SEM and TEM images of the catalysts samples of **a** and **e** Cu/ZnO, **b** and **f** Cu/ZnO/Al₂O₃, **c** and **g** Cu/ZnO/CeO₂, **d** and **h** Cu/ZnO/CeO₂@Ce-MOF, **i** and **l** Cu/ZnO/CeO₂@MOF-5, **j** and **m** Ce-MOF, **k** and **n** MOF-5

Table 2 Elemental composition of catalysts obtained from EDS analysis

Catalysts	Atomic elemental composition (%)					
	C	O	Cu	Zn	Ce	Al
Cu/ZnO	34.14	46.34	9.84	9.67	0	0
Cu/ZnO/Al ₂ O ₃	52.06	38.50	4.52	4.42	0	0.50
Cu/ZnO/CeO ₂	42.66	41.10	7.30	7.32	1.63	0
Cu/ZnO/CeO ₂ @Ce-MOF	50.64	38.06	4.26	4.64	2.41	0
Cu/ZnO/CeO ₂ @MOF-5	59.03	31.77	3.82	4.55	0.83	0
Ce-MOF	69.16	29.20	0	0	1.63	0
MOF-5	64.57	31.16	0	4.27	0	0

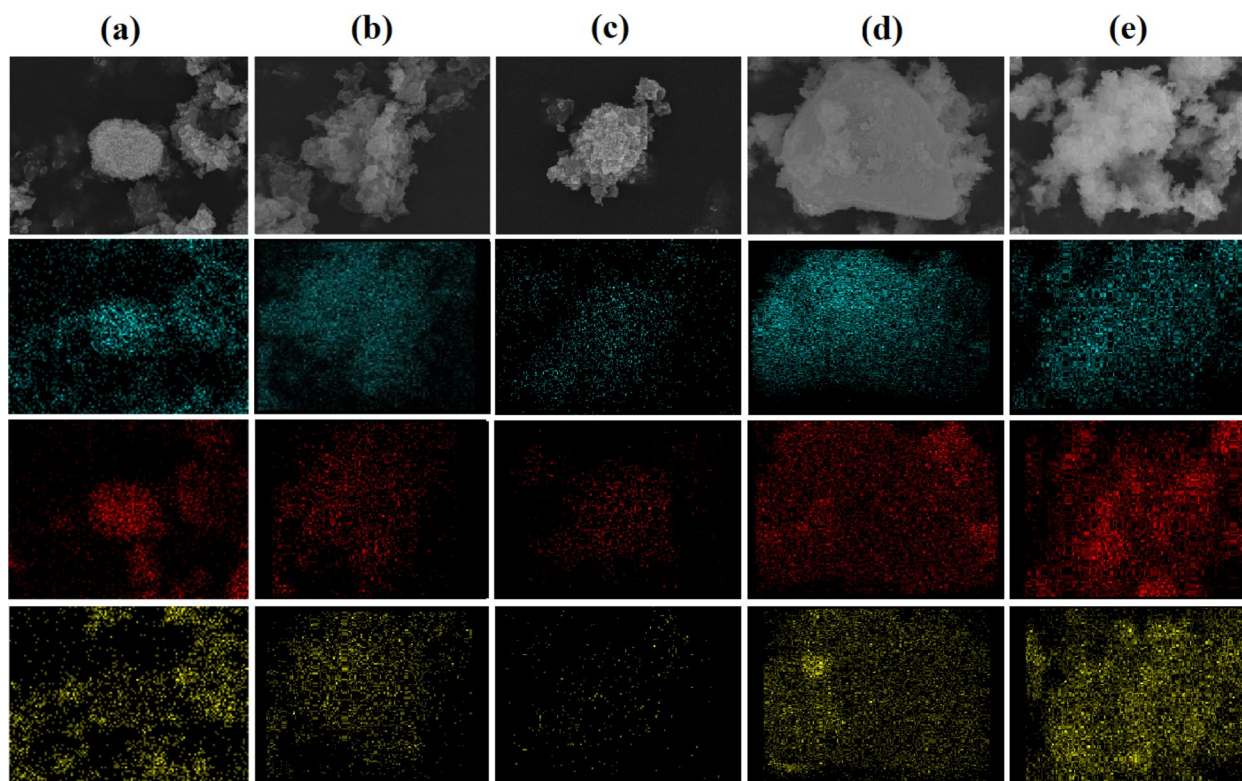


Fig. 5 EDS elemental distribution mapping of the catalysts: **a** Cu/ZnO, **b** Cu/ZnO/Al₂O₃, **c** Cu/ZnO/CeO₂, **d** Cu/ZnO/CeO₂@Ce-MOF and **e** Cu/ZnO/CeO₂@MOF-5. The colors cyan, red, and yellow represent the elements oxygen, copper and zinc, respectively

Table 3 Methanol yield (STY) results of the catalyst samples

Samples	STY (mg g _{cat} ⁻¹ h ⁻¹)			Selectivity (%)		
	(1) ^a	(2) ^b	(3) ^c	(1) ^a	(2) ^b	(3) ^c
Cu/ZnO	14.4	15.4	15.8	76	35	38
Cu/ZnO/Al ₂ O ₃	9.0	10.1	10.6	53	32	36
Cu/ZnO/CeO ₂	15.1	16.2	21.4	71	37	51
Cu/ZnO/CeO ₂ @Ce-MOF	21.3	21.8	18.3	52	36	38
Cu/ZnO/CeO ₂ @MOF-5	23.3	24.0	25.1	79	53	65
Cu/ZnO/CeO ₂ @ZIF-8C	15.9	16.7	17.1	61	43	52
Ce-MOF	0.7	0.7	0.8	90	87	89
MOF-5	1.4	1.5	1.5	93	88	90

^aThe reaction occurs at the temperature of 260 °C and pressure of 10 bar

^bThe reaction occurs at the temperature of 300 °C and pressure of 10 bar

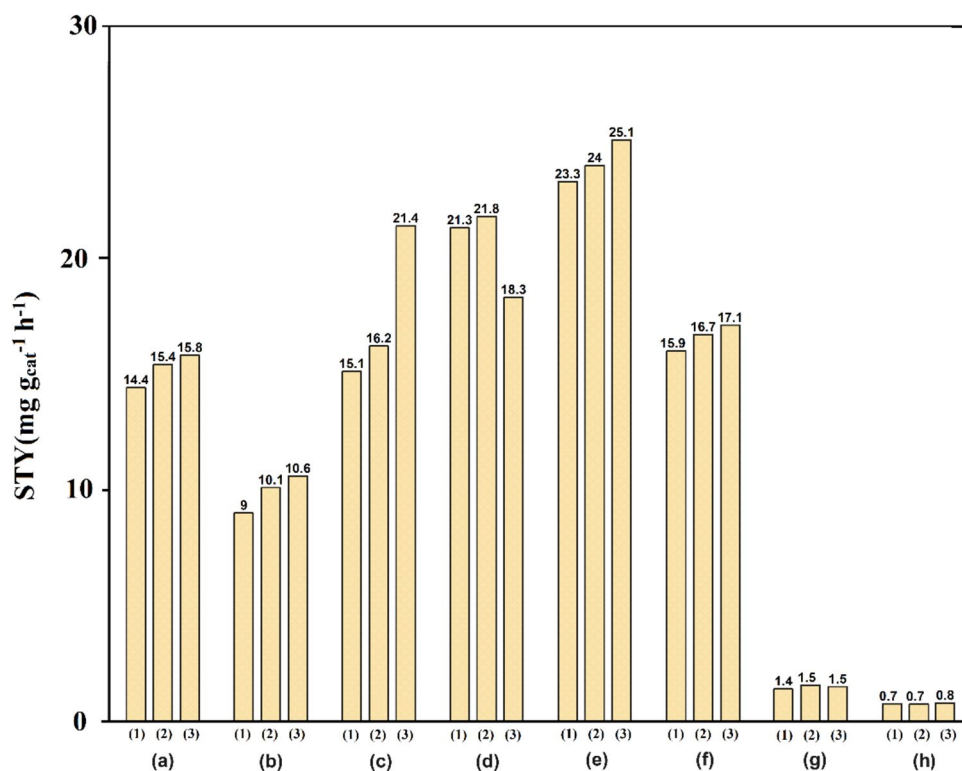
^cThe reaction occurs at the temperature of 300 °C and pressure of 15 bar

contribute to catalytic activity of nanocomposites, they do not possess the active sites for carbon dioxide to methanol hydrogenation when used individually. The mechanism of MOFs contribution to the catalytic activity will be analyzed in detail in the discussion section.

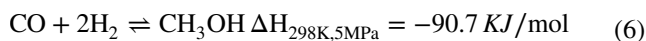
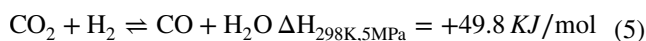
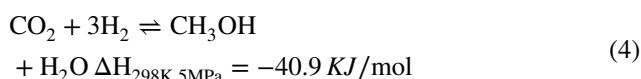
As can be observed from the STY and selectivity results, the catalytic behavior shown by all catalysts under two reaction temperatures of 260 and 300 °C indicates that with an increase in temperature, methanol STY slightly increases,

while selectivity significantly decreases (Fig. 7). Reaction pressure, on the other hand, appears to cause an increase in methanol STY and selectivity. It is known that CO₂ hydrogenation to methanol is an exothermic reaction [reaction (4)], while the competing reaction, reverse water gas shift [RWGS, reaction (5)], is endothermic. In addition, the CO produced through RWGS can go through exothermic hydrogenation to form methanol [reaction (6)] [57]. According to Le Châtelier's principle, higher pressure and lower

Fig. 6 Methanol yield (STY) results of the catalyst samples of **a** Cu/ZnO, **b** Cu/ZnO/Al₂O₃, **c** Cu/ZnO/CeO₂, **d** Cu/ZnO/CeO₂@Ce-MOF, **e** Cu/ZnO/CeO₂@MOF-5, **f** Cu/ZnO/CeO₂@ZIF-8C, **g** Ce-MOF and **h** MOF-5 at three reaction conditions: (1) Temperature 260 °C and pressure 10 bar, (2) Temperature 300 °C and pressure 10 bar and (3) Temperature 300 °C and pressure 15 bar



temperature will lead the reaction in favor of methanol formation [58]. This confirms the behavior of the catalysts used in this study as shown in Fig. 7. Taking into account that, in this study, CO was the only by-product observed of the catalytic reaction, and by increasing the temperature, CO production was increased, which can be confirmed by the selectivity results. Accordingly, with an increase of pressure from 10 to 15, methanol formation was favored and selectivity is shown to elevated:



The catalyst Cu/ZnO/CeO₂@MOF-5 was finally tested at different reactions conditions and the methanol STY, selectivity and CO₂ conversion results are displayed in Fig. 8a and b. As expected, methanol production and CO₂ conversion elevated with the increase of temperature and pressure, while selectivity was gradually decreased with temperature increase due to the dominance RWGS reaction in higher temperatures as previously mentioned. To investigate the stability of the catalyst, Cu/ZnO/CeO₂@MOF-5 was tested at 260 °C and 10 bar for 44 h of continuous reaction and

the results are presented in Fig. 8c. As observed, the catalyst demonstrated an excellent stability and maintained its catalytic activity with an insignificant decrease in methanol STY after 44 h.

4 Discussion

To date, the incorporation of different metal oxide supports with Cu/ZnO catalyst is the object of several investigations. In fact, these supports can function as structural and electronic promoters. Structural promotion refers to the fact that through metal-support interactions, the stabilization of smaller metal particles can occur, which results in more active sites [59]. Electronic promotion refers to the modification of the active sites quality, which leads to higher intrinsic activity of the active sites. The change in the contribution of different surface atom arrangements on Cu particles with different size impacts the catalytic activity since methanol synthesis is a structure-sensitive reaction [60]. Al₂O₃ as a support for Cu/ZnO catalyst has been largely investigated and commercially used. However, Cu/ZnO/Al₂O₃ showed poor performance in terms of activity and stability, which was confirmed in this study. The poor performance of Cu/ZnO/Al₂O₃ can be attributed to the strong hydrophobicity of Al₂O₃ [40], and the consequent deactivation during the hydrogenation reaction as a result of H₂O production, as shown in the reactions 4 and 5. In this study, a comparison

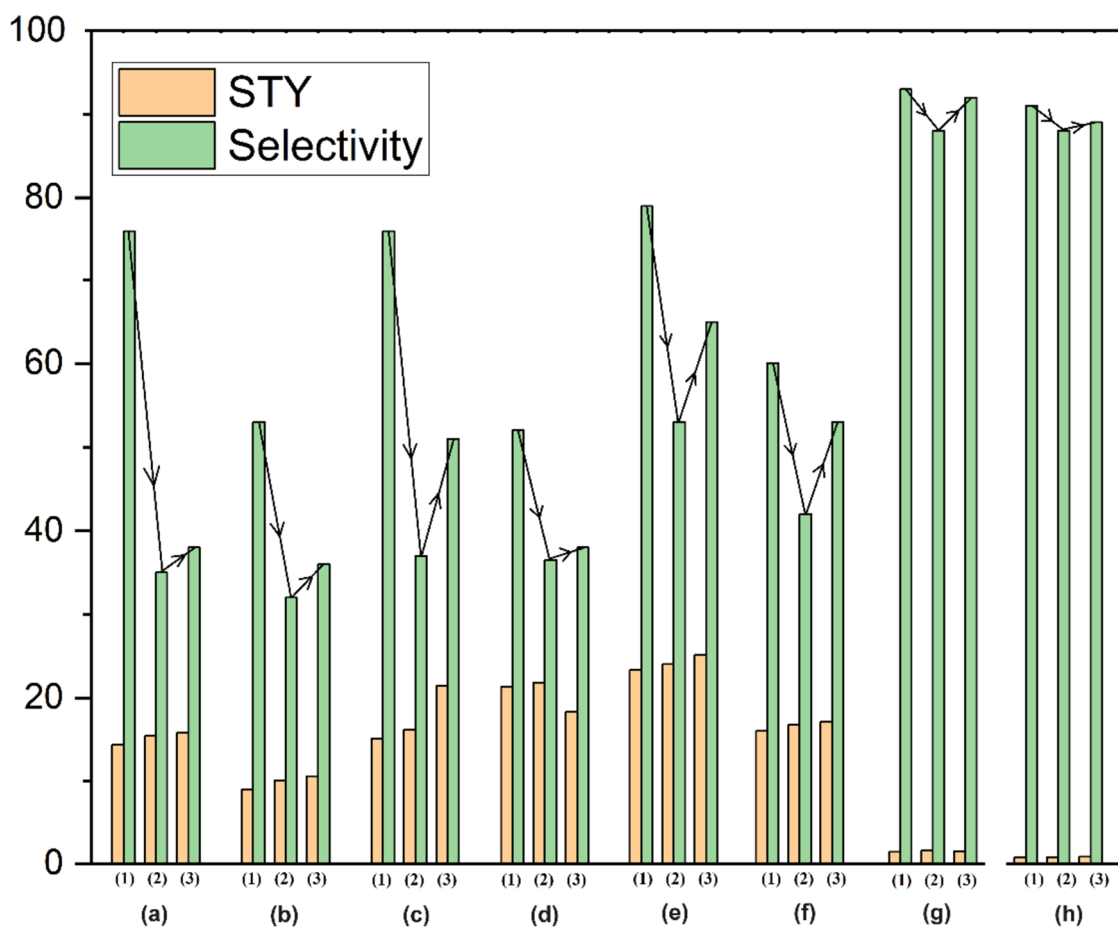


Fig. 7 Combined STY and selectivity results of the catalysts samples of **a** CuZnO, **b** CuZnOAl₂O₃, **c** CuZnOCeO₂, **d** CuZnOCeO₂@Ce-MOF, **e** CuZnOCeO₂@MOF-5, **f** CuZnOCeO₂@ZIF-8C, **g** Ce-MOF

and **h** MOF-5 at three reaction conditions: (1) Temperature 260 °C and pressure 10 bar, (2) Temperature 300 °C and pressure 10 bar, (3) Temperature 300 °C and pressure = 15 bar

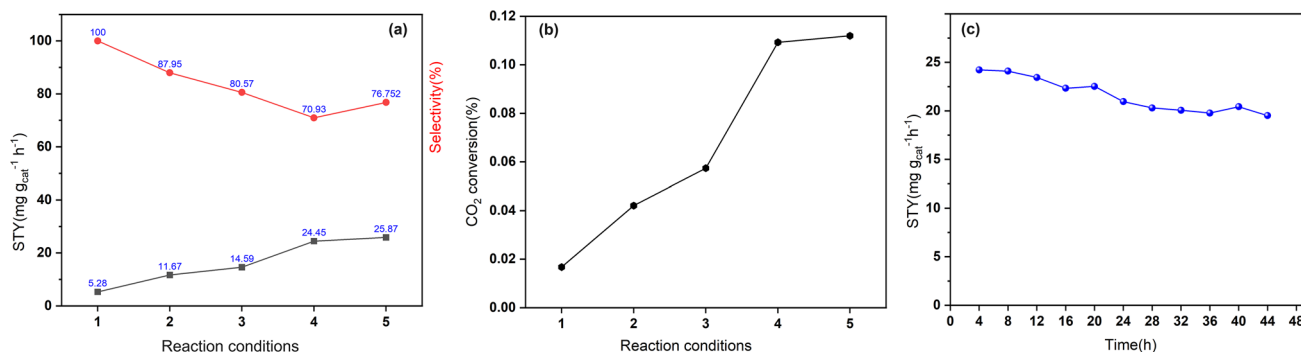


Fig. 8 **a, b** Methanol STY, selectivity, and CO₂ conversion results for the catalysts Cu/ZnO/CeO₂@MOF-5 at different reactions conditions: (1) 200 °C, 10 bar, (2) 220 °C, 10 bar, (3) 240 °C, 10 bar, (4) 260 °C,

10 bar, (5) 260 °C, 15 bar; **c** Stability results of catalyst Cu/ZnO/CeO₂@MOF-5 in terms of methanol STY

among three samples of Cu/ZnO, Cu/ZnO/Al₂O₃ and Cu/ZnO/CeO₂ in terms of methanol yield and selectivity and via characterization techniques proved the superiority of CeO₂ over Al₂O₃ as support for Cu/ZnO. CeO₂ has proved to

have strong interactions with Cu leading to higher catalytic activity of the CeO₂-supported Cu-based catalysts in CO₂ hydrogenation to methanol [61]. This is due to the fact that CeO₂ interaction with Cu enhances the Cu dispersion and

also results in the formation of oxygen vacancies on CeO₂. More oxygen vacancies enhance the binding and activation of CO₂. As it was seen in X-ray diffraction patterns corresponding to Cu/ZnO and Cu/ZnO/CeO₂, the peaks indicating the CuO and ZnO phase, were broader and less intense when the catalyst was supported by CeO₂. This demonstrates that more dispersion of CuO and ZnO occurred in case of the catalyst CuZnOCeO₂ as a result of the strong interaction that CeO₂ has with CuO and ZnO, which causes the electronic modification of Cu and Zn particles in the catalyst. This is in accordance with the specific surface area results that were reported to be 38 and 50 m²/g for Cu/ZnO and CuZnOCeO₂, respectively. The higher specific surface area of the catalyst supported with CeO₂ is clearly a result of more CuO and ZnO dispersion as well as the presence of micropores in the catalyst as shown in BET results. Furthermore, the higher dispersion of Cu and Zn in the catalyst CuZnOCeO₂ can also be clearly observed in the images obtained from EDS elemental mapping as shown in Fig. 5, as well as in SEM and TEM images illustrated in Fig. 4. SEM and TEM images of Cu/ZnO and Cu/ZnO/CeO₂ are also in agreement with the aforesaid statements and demonstrate the existence of well-dispersed CuO and ZnO due to CeO₂ support. As it was observed for Cu/ZnO samples in Fig. 4a, the nanoparticles of CuO are agglomerated in shape of spheres of 1 to 2 μm leading to improper dispersion of Cu active sites. This account for low methanol STY for Cu/ZnO compared to Cu/ZnO/CeO₂. Whereas, better Cu dispersion in the sample Cu/ZnO/CeO₂ is clearly observed in the EDS elemental mapping (Fig. 5c) as well as SEM (Fig. 4c) and TEM (Fig. 4g) images. On the other hand, the adsorption of H₂ and CO₂ and the formation of reaction intermediates over the catalyst surfaces are the crucial steps in the hydrogenation of CO₂ to methanol. In this regard, it has been reported that the metal-support interaction significantly influences the adsorption properties of reactants. For instance, Huang et al. [62] showed that these metal-support interactions in a Cu/ZnO/ZrO₂ composite provides additional active sites for the adsorption of H₂ and CO₂ under lower temperature ranges, leading to higher methanol yield [63]. Hence, apart from the electronic and structural promoting effects, metal oxide participates in the catalytic reaction through adsorbing and activating the reactants. As seen in Fig. 6, CuZnOCeO₂ gave the methanol STY of 21.4 mg g_{cat}⁻¹ h⁻¹ which is much higher than that of Cu/ZnO and commercial ternary Cu/ZnO/Al₂O₃ with methanol STYs of 15.8 and 10.6 mg g_{cat}⁻¹ h⁻¹, respectively. This is due to the catalytic activity of the reactive sites generated in the interface of Cu and CeO₂ which can adsorb and activate the CO₂ as well as higher dispersion and surface area of Cu sites in Cu/ZnO/CeO₂ rather than the commercial catalyst Cu/ZnO/Al₂O₃ and Cu/ZnO. In addition, comparing the CuO average size corresponding to the catalysts Cu/ZnO and Cu/ZnO/CeO₂ as presented in Table 1, which are 24.13

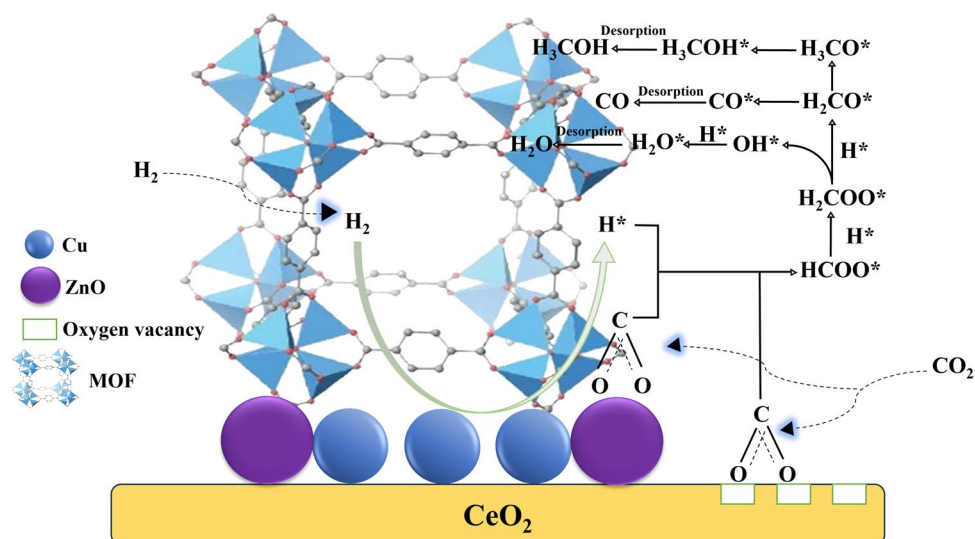
and 17.16 nm, respectively, it is confirmed that the metal-support interaction of CeO₂ with Cu leads to smaller CuO particles due to structural promotion of the support. A similar behaviour was observed when the catalyst CuZnOCeO₂ was supported on MOF-5. A comparison between methanol STY and selectivity of catalyst samples Cu/ZnO/CeO₂ and Cu/ZnO/CeO₂@MOF-5, as shown in Figs. 6 and 7, reveals that MOF-5 made a significant effect to the catalytic activity. First, the effect of MOF-5 on the Cu dispersion similarly can be explained as for CeO₂ support. In this regard, better Cu dispersion in the catalyst Cu/ZnO/CeO₂@MOF-5 is obviously observed in SEM (Fig. 4i), TEM (Fig. 4l) and EDS elemental mapping (Fig. 5e). Well-dispersed particles in Cu/ZnO/CeO₂@MOF-5 showed higher methanol STY and selectivity. Besides, the CuO average size in the catalyst Cu/ZnO/CeO₂@MOF-5 was calculated to be 15.27 nm, which is smaller than CuO average size in Cu/ZnO/CeO₂, which can be ascribed to structural promotion caused by the interaction between MOF-5 and Cu/ZnO/CeO₂. Furthermore, the interaction of metal nodes of MOF-5 with Cu, Zn and CeO₂ also helps stabilize Cu particles against sintering during the reaction, leading to high stability of the catalyst (Fig. 8).

5 Proposed Mechanism

According to the established mechanism of methanol synthesis from CO₂ hydrogenation for the commercial catalyst [30, 64–67], we propose the following mechanism for the reaction. Typically, hydrogen is adsorbed and activated on Cu surface to form H atoms (H*) [64, 68]. In this regard, since MOF-5 has a high capacity for hydrogen adsorption and storage [69], it is hypothesized that MOF-5 can also facilitates the adsorption and activation of the gas reactants. Moreover, the unsaturated Zn sites of MOF-5 can also adsorb and activate CO₂. A schematic proposed mechanism for the methanol synthesis from CO₂ hydrogenation reaction for the catalyst Cu/ZnO/CeO₂@MOF-5 is presented in Fig. 9.

As can be seen in Fig. 9, after the adsorption of hydrogen and the formation of H* atoms, H* spillover to the metal oxides across the interface between Cu and metal oxides to form the corresponding intermediates of the reaction. As mentioned before, the interaction of Cu and CeO₂ leads to higher dispersion of CuO, producing high density of Cu–CeO₂ interfaces and higher concentration of oxygen vacancies. On one hand, the binding and activation of CO₂ is favored by these interfaces [70]. On the other hand, oxygen vacancies in CeO₂ promote charge accumulation and redistribution, strengthening CO₂ adsorption and thus stabilizing the key carbonate intermediates engaged in methanol formation [71]. Then, the carbonate species react with the adjoining hydrogen atoms to form methoxide and formate, and

Fig. 9 Proposed reaction mechanism for methanol synthesis from CO₂ hydrogenation over the catalyst Cu/ZnO/CeO₂@MOF-5



eventually methanol. As observed in selectivity results, the incorporation of Ce-MOF promotes the methanol STY while leading to a decrease in selectivity of methanol. This shows that the interaction between Ce nodes of Ce-MOF with metal sites of the catalyst leads to the growth of active sites being more favorable to CO production rather than methanol. Besides, the catalyst supported by MOF-5 not only demonstrated better methanol STY than Cu/ZnO/CeO₂, but also promotes the production of methanol over CO. This can be attributed to the interaction between Zn nodes of MOF-5 and the active sites of catalyst Cu/ZnO/CeO₂, resulting in the sites which enhance the methanol production reaction via controlling the reaction intermediates in favor of methanol production. More detail information of the reaction mechanism over the catalyst Cu/ZnO/CeO₂@MOF-5 can be found through in situ diffuse reflectance infrared Fourier transform (in situ DRIFT) analysis which is recommended to be carried out in perspective studies.

6 Conclusions

Three catalysts including Cu/ZnO/CeO₂@MOF-5, Cu/ZnO/CeO₂@Ce-MOF, Cu/ZnO/CeO₂@ZIF-8 were synthesized and tested for methanol synthesis using CO₂ hydrogenation. Comparing the methanol yield and selectivity obtained for these catalysts and Cu/ZnO/CeO₂ prepared in this study, the impact of MOFs incorporation was clearly observed on the catalytic activity, which was further confirmed by characterizations results. SEM, TEM, XRD, EDS and BET analyses demonstrated the positive effect of MOF-5 as well as the effect of CeO₂ as a support for Cu/ZnO nanocomposites.

CeO₂ performed more efficiently than commercial Al₂O₃ as support, leading to higher Cu dispersion and smaller Cu size and therefore higher Cu active sites. Eventually, Cu/ZnO/CeO₂ supported on MOF-5 resulted in a higher methanol yield and selectivity, which can be explained by smaller Cu size and higher specific area for Cu/ZnO/CeO₂@MOF-5. MOF-5 and its interaction with metal and metal oxide sites of Cu/ZnO/CeO₂ and their interfaces was also assumed to contribute to the adsorption and activation of hydrogen and CO₂, leading to faster reaction kinetics and more methanol productivity. Finally, the catalyst performed well in terms of stability, showing an insignificant activity loss after 5 h of continuous reaction.

Author Contributions SAV: Writing-original draft, Conceptualization, Methodology, Formal analysis, Investigation, Writing-review & editing. JM-V: Writing-review & editing, Supervision. AS: Writing-review & editing, Supervision, Funding acquisition. XF: Writing-review & editing, Funding acquisition.

Funding Open Access Funding provided by Universitat Autònoma de Barcelona. This study was financially supported by the Spanish-Ministerio de Ciencia e Innovación in the call *Proyectos de Transición Ecológica y Transición Digital 2022. Squeezzer project, ref. TED2021-130407B-I00*.

Declarations

Competing Interests The authors declare no competing interests.

Open Access This article is licensed under a Creative Commons Attribution 4.0 International License, which permits use, sharing, adaptation, distribution and reproduction in any medium or format, as long as you give appropriate credit to the original author(s) and the source, provide a link to the Creative Commons licence, and indicate if changes were made. The images or other third party material in this article are included in the article's Creative Commons licence, unless indicated

otherwise in a credit line to the material. If material is not included in the article's Creative Commons licence and your intended use is not permitted by statutory regulation or exceeds the permitted use, you will need to obtain permission directly from the copyright holder. To view a copy of this licence, visit <http://creativecommons.org/licenses/by/4.0/>.

References

- Du S, Tang W, Lu X, Wang S, Guo Y, Gao PX (2018) Cu-decorated ZnO nanorod array integrated structured catalysts for low-pressure CO₂ hydrogenation to methanol. *Adv Mater Interfaces* 5:1700730. <https://doi.org/10.1002/admi.201700730>
- Markewitz P, Kuckshinrichs W, Leitner W, Linssen J, Zapp P, Bongartz R, Schreiber A, Müller TE (2012) Worldwide innovations in the development of carbon capture technologies and the utilization of CO₂. *Energy. Environ Sci* 5:7281–7305. <https://doi.org/10.1039/c2ee03403d>
- Arena F, Mezzatesta G, Zafarana G, Trunfio G, Frusteri F, Spadaro L (2013) Effects of oxide carriers on surface functionality and process performance of the Cu–ZnO system in the synthesis of methanol via CO₂ hydrogenation. *J Catal* 300:141–151. <https://doi.org/10.1016/j.jcat.2012.12.019>
- Vali SA, Baghdadi M, Abdoli MA (2018) Immobilization of polyaniline nanoparticles on the polyurethane foam derived from waste materials: a porous reactive fixed-bed medium for removal of mercury from contaminated waters. *J Environ Chem Eng* 6:6612–6622. <https://doi.org/10.1016/j.jece.2018.09.042>
- Leung DY, Caramanna G, Maroto-Valer MM (2014) An overview of current status of carbon dioxide capture and storage technologies. *Renew Sustain Energy Rev* 39:426–443. <https://doi.org/10.1016/j.rser.2014.07.093>
- Vali SA, Moral-Vico J, Font X, Sánchez A (2023) Adsorptive removal of siloxanes from biogas: recent advances in catalyst reusability and water content effect. *Biomass Conv Bioref*. <https://doi.org/10.1007/s13399-023-04478-1>
- Jadhav SG, Vaidya PD, Bhanage BM, Joshi JB (2014) Catalytic carbon dioxide hydrogenation to methanol: a review of recent studies. *Chem Eng Res Des* 92:2557–2567. <https://doi.org/10.1016/j.cherd.2014.03.005>
- Zhao YF, Yang Y, Mims C, Peden CHF, Li J, Mei D (2011) Insight into methanol synthesis from CO₂ hydrogenation on Cu(1 1 1): complex reaction network and the effects of H₂O. *J Catal* 281:199–211. <https://doi.org/10.1016/j.jcat.2011.04.012>
- Raudaskoski R, Turpeinen E, Lenkkeri R, Pongrácz E, Keiski RL (2009) Catalytic activation of CO₂: use of secondary CO₂ for the production of synthesis gas and for methanol synthesis over copper-based zirconia-containing catalysts. *Catal Today* 144:318–323. <https://doi.org/10.1016/j.cattod.2008.11.026>
- Rohde MP, Unruh D, Schaub G (2005) Membrane application in Fischer–Tropsch synthesis to enhance CO₂ hydrogenation. *Ind Eng Chem Res* 44:9653–9658. <https://doi.org/10.1021/ie050289z>
- Saito M, Fujitani T, Takahara I, Watanabe T, Takeuchi M, Kanai Y, Moriya K, Kakumoto T (1995) Development of Cu/ZnO-based high performance catalysts for methanol synthesis by CO₂ hydrogenation. *Energy Convers Manag* 36:577–580. [https://doi.org/10.1016/0196-8904\(95\)00071-K](https://doi.org/10.1016/0196-8904(95)00071-K)
- Toyir J, Ramírez De La Piscina P, Luis J, Fierro G, Homs N (2001) Highly effective conversion of CO₂ to methanol over supported and promoted copper-based catalysts: influence of support and promoter. *Appl Catal B Environ* 29:207–215. [https://doi.org/10.1016/S0926-3373\(00\)00205-8](https://doi.org/10.1016/S0926-3373(00)00205-8)
- Toyir J, Saito M, Yamauchi I, Luo S, Wu J, Takahara I, Takeuchi M (1998) Development of high performance Raney Cu-based catalysts for methanol synthesis from CO₂ and H₂. *Catal Today* 45:245–250. [https://doi.org/10.1016/S0920-5861\(98\)00223-5](https://doi.org/10.1016/S0920-5861(98)00223-5)
- Ma Y, Sun Q, Wu D, Fan W-H, Zhang Y-L, Deng J-F (1998) A practical approach for the preparation of high activity Cu/ZnO/ZrO₂ catalyst for methanol synthesis from CO₂ hydrogenation. *Appl Catal A Gen* 171:45–55. [https://doi.org/10.1016/S0926-860X\(98\)00079-9](https://doi.org/10.1016/S0926-860X(98)00079-9)
- Schlögl R (2015) Heterogeneous catalysis. *Angew Chem Int Ed* 54:3465–3520. <https://doi.org/10.1002/anie.201410738>
- Angelo L, Kobl K, Tejada LMM, Zimmermann Y, Parkhomenko K, Roger AC (2015) Study of CuZn MOx oxides (M = Al, Zr, Ce, CeZr) for the catalytic hydrogenation of CO₂ into methanol. *C R Chim* 18:250–260. <https://doi.org/10.1016/j.crci.2015.01.001>
- Lei H, Nie R, Wu G, Hou Z (2015) Hydrogenation of CO₂ to CH₃OH over Cu/ZnO catalysts with different ZnO morphology. *Fuel* 154:161–166. <https://doi.org/10.1016/j.fuel.2015.03.052>
- Vesborg PCK, Chorkendorff I, Knudsen I, Balmes O, Nerlov J, Molenbroek AM, Clausen BS, Helveg S (2009) Transient behavior of Cu/ZnO-based methanol synthesis catalysts. *J Catal* 262:65–72. <https://doi.org/10.1016/j.jcat.2008.11.028>
- Grunwaldt JD, Molenbroek AM, Topsøe NY, Topsøe H, Clausen BS (2000) In situ investigations of structural changes in Cu/ZnO catalysts. *J Catal* 194:452–460. <https://doi.org/10.1006/jcat.2000.2930>
- Kasatkin I, Kurr P, Kniep B, Trunschke A, Schlögl R (2007) Role of lattice strain and defects in copper particles on the activity of Cu/ZnO/Al₂O₃ catalysts for methanol synthesis. *Angew Chem Int Ed* 46:7324–7327. <https://doi.org/10.1002/anie.200702600>
- Hansen PL, Wagner JB, Helveg S, Rostrup-Nielsen JR, Clausen BS, Topsøe H (2002) Atom-resolved imaging of dynamic shape changes in supported copper nanocrystals. *Science* 295:2053–2055. <https://doi.org/10.1126/science.1069325>
- Naumann R, D'Alnoncourt X, Xia J, Strunk E, Löffler O, Hinrichsen M (2006) Muhler, The influence of strongly reducing conditions on strong metal-support interactions in Cu/ZnO catalysts used for methanol synthesis. *Phys Chem Chem Phys* 8:1525–1538. <https://doi.org/10.1039/b515487a>
- Batyrev ED, Van Den Heuvel JC, Beckers J, Jansen WPA, Castriem HL (2005) The effect of the reduction temperature on the structure of Cu/ZnO/SiO₂ catalysts for methanol synthesis. *J Catal* 229:136–143. <https://doi.org/10.1016/j.jcat.2004.10.012>
- Studt F, Behrens M, Kunkes EL, Thomas N, Zander S, Tarasov A, Schumann J, Frei E, Varley JB, Abild-Pedersen F, Nørskov JK, Schlögl R (2015) The mechanism of CO and CO₂ hydrogenation to methanol over Cu-based catalysts. *ChemCatChem* 7:1105–1111. <https://doi.org/10.1002/cctc.201500123>
- Behrens M, Studt F, Kasatkin I, Kühl S, Hävecker M, Abild-Pedersen F, Zander S, Girgsdies F, Kurr P, Kniep B-L, Tovar M, Fischer RW, Nørskov JK, Schlögl R (2012) The active site of methanol synthesis over Cu/ZnO/Al₂O₃ industrial catalysts. *Science* 336:893–897. <https://doi.org/10.1126/science.1219831>
- Behrens M (2016) Promotierungseffekte in der methanolsynthese: verständnis eines industriellen katalysators für die umsetzung von CO₂. *Angew Chem* 128:15128–15130. <https://doi.org/10.1002/ange.201607600>
- Liang B, Ma J, Su X, Yang C, Duan H, Zhou H, Deng S, Li L, Huang Y (2019) Investigation on deactivation of Cu/ZnO/Al₂O₃ catalyst for CO₂ hydrogenation to methanol. *Ind Eng Chem Res* 58:9030–9037. <https://doi.org/10.1021/acs.iecr.9b01546>
- Prašnikar A, Pavlišić A, Ruiz-Zepeda F, Kovač J, Likozar B (2019) Mechanisms of copper-based catalyst deactivation during CO₂ reduction to methanol. *Ind Eng Chem Res* 58:13021–13029. <https://doi.org/10.1021/acs.iecr.9b01898>
- Wu J, Saito M, Takeuchi M, Watanabe T (2001) The stability of Cu/ZnO-based catalysts in methanol synthesis from a CO₂-rich

- feed and from a CO-rich feed. *Appl Catal A Gen* 218:235–240. [https://doi.org/10.1016/S0926-860X\(01\)00650-0](https://doi.org/10.1016/S0926-860X(01)00650-0)
30. Larmier K, Liao W-C, Tada S, Lam E, Verel R, Bansode A, Urakawa A, Comas-Vives A, Cop  t C (2017) CO₂-to-methanol hydrogenation on zirconia-supported copper nanoparticles: reaction intermediates and the role of the metal-support interface. *Angew Chem* 129:2358–2363. <https://doi.org/10.1002/ange.201610166>
 31. Fisher IA, Woo HC, Bell AT (1997) Effects of zirconia promotion on the activity of Cu/SiO₂ for methanol synthesis from CO/H₂ and CO₂/H₂. *Catal Lett* 44:11–17. <https://doi.org/10.1023/A:1018916806816>
 32. Shi Z, Tan Q, Wu D (2019) Enhanced CO₂ hydrogenation to methanol over TiO₂ nanotubes-supported CuO–ZnO–CeO₂ catalyst. *Appl Catal A Gen* 581:58–66. <https://doi.org/10.1016/j.apcata.2019.05.019>
 33. Shi Z, Tan Q, Tian C, Pan Y, Sun X, Zhang J, Wu D (2019) CO₂ hydrogenation to methanol over Cu–In intermetallic catalysts: effect of reduction temperature. *J Catal* 379:78–89. <https://doi.org/10.1016/j.jcat.2019.09.024>
 34. Chen K, Fang H, Wu S, Liu X, Zheng J, Zhou S, Duan X, Zhuang Y (2019) CO₂ hydrogenation to methanol over Cu catalysts supported on La-modified SBA-15: the crucial role of Cu–LaO_x interfaces. *Appl Catal B Environ* 251:119–129. <https://doi.org/10.1016/j.apcatb.2019.03.059>
 35. Xu W, Ram  rez PJ, Stacchiola D, Brito JL, Rodr  guez JA (2015) The carburization of transition metal molybdates (M_xMoO₄, M = Cu, Ni or Co) and the generation of highly active metal/carbide catalysts for CO₂ hydrogenation. *Catal Lett* 145:1365–1373. <https://doi.org/10.1007/s10562-015-1540-5>
 36. Chen K, Duan X, Fang H, Liang X, Yuan Y (2018) Selective hydrogenation of CO₂ to methanol catalyzed by Cu supported on rod-like La₂O₃CO₃. *Catal Sci Technol* 8:1062–1069. <https://doi.org/10.1039/c7cy01998j>
 37. Sripada P, Kimpton J, Barlow A, Williams T, Kandasamy S, Bhat-tacharya S (2020) Investigating the dynamic structural changes on Cu/CeO₂ catalysts observed during CO₂ hydrogenation. *J Catal* 381:415–426. <https://doi.org/10.1016/j.jcat.2019.11.017>
 38. Wang W, Qu Z, Song L, Fu Q (2020) CO₂ hydrogenation to methanol over Cu/CeO₂ and Cu/ZrO₂ catalysts: tuning methanol selectivity via metal-support interaction. *J Energy Chem* 40:22–30. <https://doi.org/10.1016/j.jechem.2019.03.001>
 39. Zhu J, Ciolca D, Liu L, Parastaev A, Kosinov N, Hensen EJM (2021) Flame synthesis of Cu/ZnO–CeO₂ catalysts: synergistic metal-support interactions promote CH₃OH selectivity in CO₂ hydrogenation. *ACS Catal* 11:4880–4892. <https://doi.org/10.1021/acscatal.1c00131>
 40. Guo J, Luo Z, Hu GT, Wang Z (2021) Synthesis of oxygen vacancies enriched Cu/ZnO/CeO₂ for CO₂ hydrogenation to methanol. *Greenh Gas Sci Technol* 11:1171–1179. <https://doi.org/10.1002/ghg.2102>
 41. Wang Q, Astruc D (2020) State of the art and prospects in metal-organic framework (MOF)-based and MOF-derived nanocatalysis. *Chem Rev* 120:1438–1511. <https://doi.org/10.1021/acs.chemrev.9b00223>
 42. Vali SA, Markeb AA, Moral-Vico J, Font X, S  nchez A (2023) Recent advances in the catalytic conversion of methane to methanol: from the challenges of traditional catalysts to the use of nanomaterials and metal-organic frameworks. *Nanomaterials* 13:2754. <https://doi.org/10.3390/nano13202754>
 43. Zhou C, Nan YY, Zha F, Tian HF, Tang XH, Chang Y (2021) Application of metal–organic frameworks in CO₂ hydrogenation. *J Fuel Chem Technol* 49:1444–1457. [https://doi.org/10.1016/S1872-5813\(21\)60097-X](https://doi.org/10.1016/S1872-5813(21)60097-X)
 44. Olajire AA (2018) Synthesis chemistry of metal–organic frameworks for CO₂ capture and conversion for sustainable energy future. *Renew Sustain Energy Rev* 92:570–607. <https://doi.org/10.1016/j.rser.2018.04.073>
 45. An B, Zhang J, Cheng K, Ji P, Wang C, Lin W (2017) Confinement of ultrasmall Cu/ZnOx nanoparticles in metal-organic frameworks for selective methanol synthesis from catalytic hydrogenation of CO₂. *J Am Chem Soc* 139:3834–3840. <https://doi.org/10.1021/jacs.7b00058>
 46. Yang Y, Xu Y, Ding H, Yang D, Cheng E, Hao Y, Wang H, Hong Y, Su Y, Wang Y, Peng L, Li J (2021) Cu/ZnOx@UiO-66 synthesized from a double solvent method as an efficient catalyst for CO₂ hydrogenation to methanol. *Catal Sci Technol* 11:4367–4375. <https://doi.org/10.1039/d0cy02450c>
 47. Rungtaweeworani B, Baek J, Araujo JR, Archanjo BS, Choi KM, Yaghi OM, Somorjai GA (2016) Copper nanocrystals encapsulated in Zr-based metal–organic frameworks for highly selective CO₂ hydrogenation to methanol. *Nano Lett* 16:7645–7649. <https://doi.org/10.1021/acs.nanolett.6b03637>
 48. Chen B, Wang X, Zhang Q, Xi X, Cai J, Qi H, Shi S, Wang J, Yuan D, Fang M (2010) Synthesis and characterization of the interpenetrated MOF-5. *J Mater Chem* 20:3758–3767. <https://doi.org/10.1039/b922528e>
 49. Zhao H, Song H, Chou L (2012) Nickel nanoparticles supported on MOF-5: synthesis and catalytic hydrogenation properties. *Inorg Chem Commun* 15:261–265. <https://doi.org/10.1016/j.inoche.2011.10.040>
 50. Vali SA, Markeb AA, Moral-Vico J, Font X, S  nchez A (2023) A novel Cu-based catalyst supported in chitosan nanoparticles for the hydrogenation of carbon dioxide to methanol: from the optimization of the catalyst performance to the reaction mechanism. *Catal Commun* 182:106747. <https://doi.org/10.1016/j.catcom.2023.106747>
 51. Yoshio K, Onodera A, Satoh H, Sakagami N, Yamashita H (2001) Crystal structure of ZnO: Li at 293 K and 19 K by X-ray diffraction. *Ferroelectrics* 264:133–138. <https://doi.org/10.1080/00150190108008559>
 52. Bellotto M, Rebours B, Clause O, Lynch J, Bazin D, Elkar E (1996) Hydrotalcite decomposition mechanism: a clue to the structure and reactivity of spinel-like mixed oxides. *J Phys Chem* 100:8535–8542. <https://doi.org/10.1021/jp960040i>
 53. Montanari T, Sisani M, Nocchetti M, Vivani R, Delgado MCH, Ramis G, Busca G, Costantino U (2010) Zinc–aluminum hydrotalcites as precursors of basic catalysts: preparation, characterization and study of the activation of methanol. *Catal Today* 152:104–109. <https://doi.org/10.1016/j.cattod.2009.09.012>
 54. Yashima M, Kobayashi S, Yasui T (2006) Crystal structure and the structural disorder of ceria from 40 to 1497   C. *Solid State Ion* 177:211–215. <https://doi.org/10.1016/j.ssi.2005.10.033>
 55. Lin A, Ibrahim AA, Arab P, El-Kaderi HM, El-Shall MS (2017) Palladium nanoparticles supported on Ce-metal-organic framework for efficient CO oxidation and low-temperature CO₂ capture. *ACS Appl Mater Interfaces* 9:17961–17968. <https://doi.org/10.1021/acsami.7b03555>
 56. Li B, Wang F, Li K, Ning P, Chen M, Zhang C (2023) CeO₂-supported Fe, Co and Ni toward CO₂ hydrogenation: tuning catalytic performance via metal-support interaction. *J Rare Earths* 41:926–932. <https://doi.org/10.1016/j.jre.2023.02.009>
 57. Gaikwad R, Bansode A, Urakawa A (2016) High-pressure advantages in stoichiometric hydrogenation of carbon dioxide to methanol. *J Catal* 343:127–132. <https://doi.org/10.1016/j.jcat.2016.02.005>
 58. Skrzypek J, Lachowska M, Grzesik M (1995) Thermodynamics and kinetics of low pressure methanol synthesis. *Chem Eng J Biochem Eng J* 58:101–108. [https://doi.org/10.1016/0923-0467\(94\)02955-5](https://doi.org/10.1016/0923-0467(94)02955-5)
 59. Parastaev A, Muravev V, Huertas Osta E, van Hoof AJF, Kimpel TF, Kosinov N, Hensen EJM (2020) Boosting CO₂ hydrogenation

- via size-dependent metal–support interactions in cobalt/ceria-based catalysts. *Nat Catal.* 3:526–533. <https://doi.org/10.1038/s41929-020-0459-4>
60. Van Den Berg R, Prieto G, Korpershoek G, Van Der Wal LI, Van Bunningen AJ, Lægsgaard-Jørgensen S, De Jongh PE, De Jong KP (2016) Structure sensitivity of Cu and CuZn catalysts relevant to industrial methanol synthesis. *Nat Commun* 7:13057. <https://doi.org/10.1038/ncomms13057>
 61. Nix RM, Lambert RM, Robertjennings J, Owen A (1987) An in situ X-ray diffraction study of the activation and performance of methanol synthesis catalysts derived from rare earth-copper alloys. *J catal* 106:216–234. [https://doi.org/10.1016/0021-9517\(87\)90226-0](https://doi.org/10.1016/0021-9517(87)90226-0)
 62. Huang C, Chen S, Fei X, Liu D, Zhang Y (2015) Catalytic hydrogenation of CO₂ to methanol: study of synergistic effect on adsorption properties of CO₂ and H₂ in CuO/ZnO/ZrO₂ system. *Catalysts* 5:1846–1861. <https://doi.org/10.3390/catal5041846>
 63. Arena F, Italiano G, Barbera K, Bordiga S, Bonura G, Spadaro L, Frusteri F (2008) Solid-state interactions, adsorption sites and functionality of Cu–ZnO/ZrO₂ catalysts in the CO₂ hydrogenation to CH₃OH. *Appl Catal A Gen* 350:16–23. <https://doi.org/10.1016/j.apcata.2008.07.028>
 64. Gao P, Li F, Zhang L, Zhao N, Xiao F, Wei W, Zhong L, Sun Y (2013) Influence of fluorine on the performance of fluorine-modified Cu/Zn/Al catalysts for CO₂ hydrogenation to methanol. *J CO₂ Util* 2:16–23. <https://doi.org/10.1016/j.jcou.2013.06.003>
 65. Fisher IA, Bell AT (1998) In-situ infrared study of methanol synthesis from H₂/CO over Cu/SiO₂ and Cu/ZrO₂/SiO₂. *J Catal* 178:153–173. <https://doi.org/10.1006/jcat.1998.2134>
 66. Yoshihara J, Campbell CT (1995) Methanol synthesis and reverse water–gas shift kinetics over Cu(110) model catalysts: structural sensitivity. *Catal Lett* 31:313–324. <https://doi.org/10.1007/BF00808595>
 67. Chen C-S, Cheng W-H, Lin S-S (2003) Study of reverse water gas shift reaction by TPD, TPR and CO₂ hydrogenation over potassium-promoted Cu/SiO₂ catalyst. *Appl Catal A Gen* 238:55–67. [https://doi.org/10.1016/S0926-860X\(02\)00221-1](https://doi.org/10.1016/S0926-860X(02)00221-1)
 68. Phongamwong T, Chantaprasertporn U, Witoon T, Numpilai T, Poo-arporn Y, Limphirat W, Donphai W, Dittanet P, Chareonpanich M, Limtrakul J (2017) CO₂ hydrogenation to methanol over CuO–ZnO–ZrO₂–SiO₂ catalysts: effects of SiO₂ contents. *Chem Eng J* 316:692–703. <https://doi.org/10.1016/j.cej.2017.02.010>
 69. Rosi NL, Eckert J, Eddaoudi M, Vodak DT, Kim J, Yaghi OM (2003) Hydrogen storage in microporous metal–organic frameworks. *Science* 300:1127–1129. <https://doi.org/10.1126/science.1083440>
 70. Senanayake SD, Ramírez PJ, Waluyo I, Kundu S, Mudiyansele K, Liu Z, Liu Z, Axnanda S, Stacchiola DJ, Evans J, Rodriguez JA (2016) Hydrogenation of CO₂ to methanol on CeO_x/Cu(111) and ZnO/Cu(111) catalysts: role of the metal–oxide interface and importance of Ce³⁺ sites. *J Phys Chem C* 120:1778–1784. <https://doi.org/10.1021/acs.jpcc.5b12012>
 71. Kattel S, Liu P, Chen JG (2017) Tuning selectivity of CO₂ hydrogenation reactions at the metal/oxide interface. *J Am Chem Soc* 139:9739–9754. <https://doi.org/10.1021/jacs.7b05362>

Publisher's Note Springer Nature remains neutral with regard to jurisdictional claims in published maps and institutional affiliations.